Chinese Chemical Letters 35 (2024) 108532

Contents lists available at ScienceDirect

Chinese Chemical Letters

journal homepage: www.elsevier.com/locate/cclet

Highly sensitive Fe^{3+} luminescence detection *via* single-ion adsorption

Yujing Li[a], Xiaojun Zhang[a], Zicheng Wang[a], Lina Zhao[a,b], Yuxin Li[a,*]

[a] *Key Laboratory of Function Inorganic Material Chemistry (MOE), School of Chemistry and Material Science, and School of Civil Engineering, Heilongjiang University, Harbin 150080, China*

[b] *Department of Food & Environmental Engineering, East University of Heilongjiang, Harbin 150066, China*

ARTICLE INFO

Article history:
Received 27 March 2023
Revised 13 April 2023
Accepted 29 April 2023
Available online 2 May 2023

Keywords:
Luminescence detection
Lanthanide complex
High sensitivity
Fe^{3+} ion
Single-ion adsorption

ABSTRACT

To achieve a lower detection limit has always been a goal of analytical chemists. Herein, we demonstrate the first picomolar level detection capability for Fe^{3+} ion *via* luminescence detection technology. The results of structural analysis and theoretical calculation show that Fe^{3+} ions are adsorbed on the central node of Eu-DBM (DBM = dibenzoylmethane) sensor in the form of single ion at ultralow concentration. Subsequently, the pathways of photo-induced charge and energy transfer of the obtained Eu-DBM@Fe^{3+} material have been changed, from the initial DBM-to-Eu^{3+} before Fe^{3+} adsorption to the ultimate DBM-to-Fe^{3+} after adsorption process, which quenches the luminescence of Eu^{3+} ion. This work not only obtains the highly sensitive luminescence detection ability, but also innovatively proposes the single-ion adsorption mechanism, both of which have important scientific and application values for the development of more efficient detection agents in the future.

Ferric ion (Fe^{3+}) is indispensable to living organisms because of its importance in hemoglobin formation, oxygen absorption, and DNA/RNA synthesis [1–4]. For clarifying the Fe^{3+}effect in physiological system, it is necessary to conduct ultrasensitive quantitative analysis of Fe^{3+} ion, preferably to achieve the detection capability at single-molecule level (10^{-15}–10^{-12} mol/L). To achieve this goal, analytical chemists have developed a series of techniques up to now. However, it is difficult for these physical and chemical detection techniques to work in the biomedical field. Luminescence detection is a promising technology effectively combining chemical detection and biomedical mechanism analysis, which is conducive to realize the chemical detection by monitoring the luminescence intensity, then to observe the dynamic mechanism of analytes in cells through confocal imaging methodology [5–7]. Although subnanomolar level Fe^{3+} detection has been realized by now [8], it is still difficult and requirable for single-molecule detection at the picomolar (pmol/L) level.

Traditionally, the luminescence detection behavior is generally realized by inner filter effect and/or Förster resonance energy transfer mechanism [9,10]. However, the non-immediately contact between sensor and analyte confines the sensitivity, because of many environmental factors. Therefore, an adsorption strategy is necessary for realizing the ultrasensitive detection, in which the analyte directly changes the energy/charge transfer pathways of the luminescence sensor at close range. Based on this consideration, a luminescent lanthanide complex, $(HNEt_3)^+[Eu(DBM)_4]^-$ (DBM = dibenzoylmethane, denoted as Eu-DBM), is selected as the sensor because of its excellent luminescence performance and exceptional water-induced luminescence improvement phenomenon [11]. More importantly, its paddle-like molecular structure and open Eu-O nodes provide an ideal platform for Fe^{3+} ion adsorption.

The Eu-DBM was synthesized by following the protocols previously reported [11] (Figs. S1–S6 in Supporting information). Upon the excitation from 365 nm, its 1 g/L well-dispersed aqueous suspension kept the intense luminescent emission at 614 nm corresponding to the electric dipole transition ($^5D_0 \rightarrow {}^7F_2$), comparable to the solid-state sample (Fig. S7 in Supporting information). This rendered stable and intense red-light emission with the Commission Internationale de L'Eclairage (CIE) coordination of (0.648, 0.330) [12] (Fig. S8 in Supporting information). In addition, the complex-maintained luminescence intensity of more than 80% under the conditions of pH 5–11 or temperature 0–90 °C. Its aqueous suspension also ensured that the solid does not settle within 48 h, and the luminescence intensity remained above 90%. The above experimental results proved the good stability at solid state and in the aqueous suspension of the Eu-DBM complex (Figs. S9–S14 in Supporting information).

Then, the Eu-DBM as a sensor was mixed with isometric aqueous solution containing 0.01 mol/L concentration of various common metal cations in human physical system. According to Figs.

* Corresponding author.
E-mail address: liyuxin@hlju.edu.cn (Y. Li).

https://doi.org/10.1016/j.cclet.2023.108532
1001-8417/

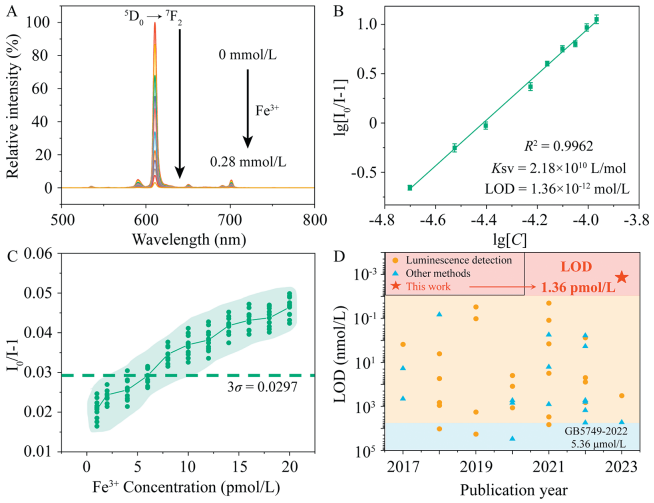

Fig. 1. (A) The concentration-dependence luminescence spectra of Eu-DBM toward Fe^{3+}; (B) The SV plot of Eu-DBM toward Fe^{3+}; (C) Fluorescence intensity of 1 g/L Eu-DBM sensor containing low concentration Fe^{3+} ions (1–20 pmol/L); (D) The limit of detection towards Fe^{3+} ions were compared with the literature results reported in the previous 7 years.

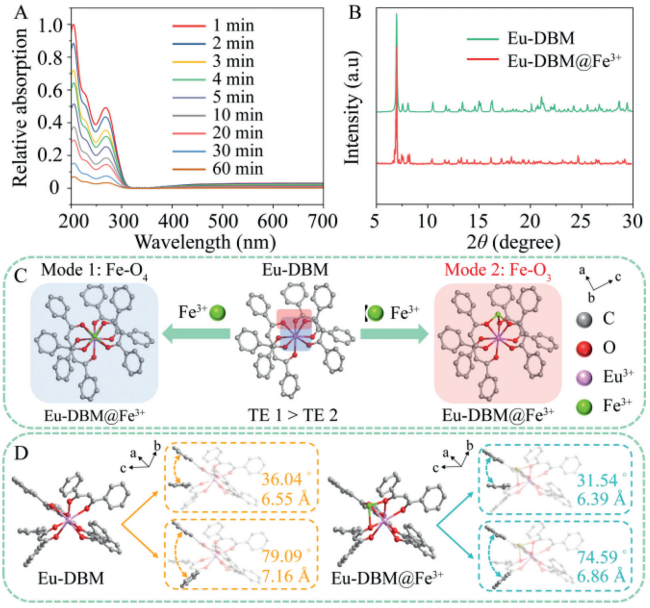

Fig. 2. (A) The UV–vis spectra of the filtrate of Eu-DBM nanocrystals immersed in 20 nmol/L Fe^{3+} solution for 1 h; (B) PXRD patterns of Eu-DBM before and after detecting Fe^{3+} cation; (C) Structural schemes of Eu-DBM@Fe^{3+} after geometric optimization of Materials Studio 2017 software (TE = Total energy); (D) The geometric optimization structure of Eu-DBM before (left) and after (right) adsorption of Fe^{3+} ions. H and $(HNEt_3)^+$ are transparent.

S15 and S16 (Supporting information), Fe^{3+} ion yielded obvious luminescent quenching to the sensor, while others only occurred negligible alternation on luminescence intensity. As shown in Fig. 1A, the luminescent intensity of the sensor was dramatically quenched as the increasing Fe^{3+} concentration, featuring heavy concentration dependence behavior. The depicted Stern-Volmer (SV) plot conformed to a double- logarithmic relationship between the quenching efficiency (I_0/I-1) and Fe^{3+} concentration (Fig. 1B) [13–16]. As a result, the K_{SV} and limit of detection (LOD) were determined as 2.18 × 10^{10} L/mol and 1.36 × 10^{-12} mol/L, respectively. According to these results, the Eu-DBM complex demonstrated pmol/L level detection capability toward Fe^{3+} ion. Moreover, it represented eminent competitiveness and recyclability (Figs. S17–S19 in Supporting information).

Although the above fitting analyses showed that the Eu-DBM complex possesses pmol/L level detection ability for Fe^{3+}, it was suspicious whether it exhibited such low detection ability in real sample of low Fe^{3+} concentration. In view of this, we used dilution method to prepare a series of Fe^{3+} aqueous solution with pmol/L level concentration. They were dripped into Eu-DBM aqueous solution sensor respectively to test the luminescence quenching of Eu^{3+} ion. As shown in Fig. 1C, when the concentration of Fe^{3+} ion was larger than 5 × 10^{-12} mol/L, the quenching coefficient began to be higher than the value of 3σ (σ is the standard deviation of the luminescence intensity at 614 nm for three groups repeated blank luminescent measurements, the specific values are listed in Table S1 in Supporting information) [17–22], indicating that the detection capability took effect. Based on this, we judged that the pmol/L level Fe^{3+} detection has been realized even in the real-sample tests, prior the previous reports. (Fig. 1D and Table S2 in Supporting information). Furthermore, the pH values of the suspension were 6.88 and 6.38 before and after introducing 20 pmol/L Fe^{3+} ions, respectively. The acidity was within the stability range of the complex, suggesting that the introduction of Fe^{3+} ion will not damage the structure of the complex due to the increment of systematic acidity.

Given that Eu-DBM has an anionic skeleton structure, we hypothesized that there was a strong adsorption capacity of Eu-DBM to Fe^{3+} cations at low concentration. To verify this hypothesis, we soaked Eu-DBM nanocrystal into 20 nmol/L Fe^{3+} aqueous solution for 1 h Although a series of data confirmed the existence of Fe^{3+} (Fig. 2A, Fig. S20 and Table S3 in Supporting information), undiscernible Fe aggregation nanoparticles could be observed according to the PXRD patterns and SEM images (Fig. 2B and Fig. S21 in Supporting information). These suggested that Fe^{3+} ion was adsorbed by Eu-DBM in a highly dispersed single-ion state rather than aggregation state. Generally, this kind of single-ion or single-atom adsorption can be confirmed by means of special aberration corrected transmission electron microscope and synchrotron radiation technologies. However, due to the particularity of Eu^{3+} ion in the outer 4f electron and Fe^{3+} in the spin polarization, the above methods cannot work. Therefore, theoretical calculation was forced to determine the adsorption behavior of Eu-DBM for Fe^{3+} ion. According to the results of structural optimization and energy calculation, the Fe^{3+} ion was preferably adsorbed onto the central Eu-O_8 node with two probable modes: (1) Fe-O_4 mode where Fe attached to the above or below plane of the distorted square-antiprismatic geometry (mode 1 in Fig. 2C); (2) Fe-O_3 mode where Fe attached to the sides of the distorted square-antiprismatic geometry (mode 2 in Fig. 2C). The total energy of Fe-O_3 was slight lower than that of Fe-O_4 (Table S4 in Supporting information). In addition, the structure of Eu-DBM after Fe^{3+} adsorption also changed: dihedral angle between the two benzene rings of the molecule was reduced (Fig. 2D). This was beneficial to the conjugation and charge transfer between benzene rings and hindered the charge transfer of benzene ring to central Eu^{3+} ions, both of which affected the energy transfer and leading to luminescence quenching. To verify this hypothesis, we conducted further analyses of the detection mechanism.

Lowest unoccupied molecular orbital (LUMO) and highest occupied molecular orbital (HOMO) energy levels, as well as the corresponding frontier orbitals for Eu-DBM and Eu-DBM@Fe^{3+}, were calculated, which showed the potential of the existence of electron transfer (Fig. 3A). The differential charge of Eu-DBM complex molecules before and after adsorption of Fe^{3+} single ion further confirmed the above hypothesis (Fig. 3B). The UV–vis spectra of Eu-DBM suspension found that the UV absorption edge of Eu-DBM@Fe^{3+} was red-shifted, and simultaneously obvious tail ab-

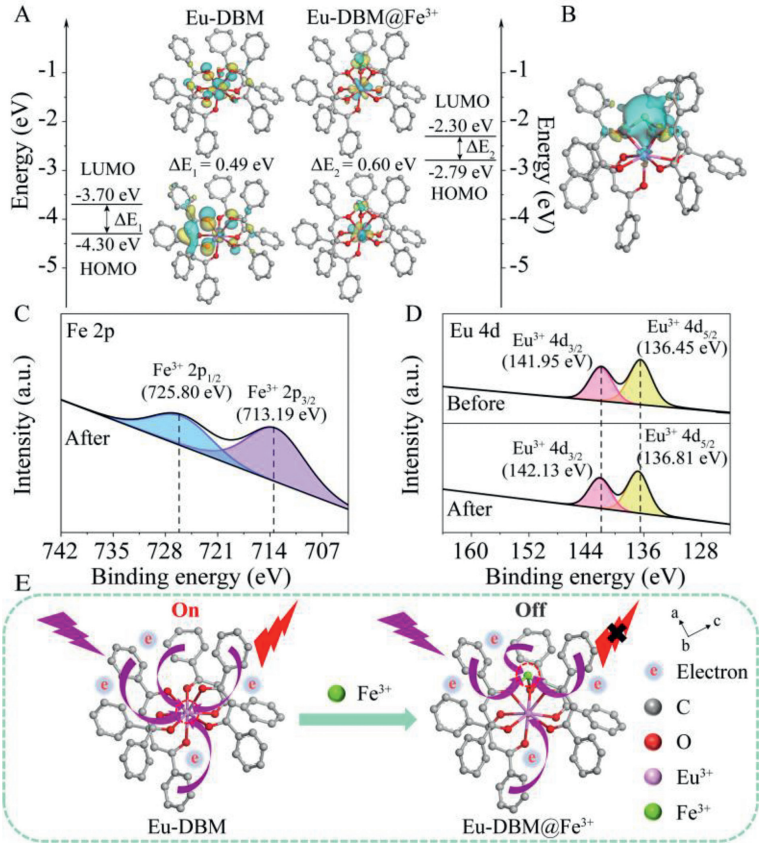

Fig. 3. (A) The optimized geometry of Eu-DBM@Fe^{3+} and frontier orbitals of Eu-DBM and Eu-DBM@Fe^{3+}. (B) Differential charge analysis of Eu-DBM@Fe^{3+}; XPS spectra before and after Fe^{3+} adsorption of Eu-DBM for Fe 2p (C) and Eu 4d (D). (E) Charge transfer diagram before and after Eu-DBM detection of Fe^{3+} ion.

sorption (Urbach tail) appeared (Fig. S22 in Supporting information) [23,24]. This long-wavelength absorption tail (>400 nm) was caused by the charge transfer interaction between the Eu-DBM donor and the Fe^{3+} acceptor [25].

The appearance of Fe 2p signal in the XPS scan confirmed the presence of Fe^{3+} adsorbed on the surface of Eu-DBM (Fig. 3C and Fig. S23 in Supporting information). It can be seen from Fig. S24 that the O 1s high-resolution spectrum of Eu-DBM was divided into two peaks at 530.53 eV and 532.55 eV, which were attributed to metal-bound ionic bonds (Eu-O) and hydroxyl groups (Eu-OH) [26]. After adsorption, the binding energy of Eu-O and Eu-OH increased, indicating that a chemical bond was formed between Fe^{3+} and Eu-O. This resulted from the electron transfer from the extranuclear electrons of O to the unoccupied orbital of Fe^{3+}, resulting in a decrease in the density of the extranuclear electron cloud. Subsequently, the weakening of O nuclear shielding enhanced the attraction between O 1s electrons and target ions. In addition, the change of the electron cloud distribution of O will cause the shift of Eu-O shared electrons, resulting in the shift of Eu 4d binding energy (Fig. 3D). It was worth noting that these peaks in Eu-DBM@Fe^{3+} samples all shifted to higher binding energies, indicating that strong ionic bonds (Fe-O) were the reason for the effective adsorption of Fe^{3+} on Eu-DBM [27]. The above results certified that the electron transfer from benzene rings to the central Eu^{3+} ion was greatly inhibited after adsorbing Fe^{3+} ion (Fig. 3E) [28]. This explained that the Fe^{3+} adsorption as single-ion formation reduced the charge supply to Eu^{3+}, and further affected its luminescence. Furthermore, the energy difference between the triplet-state DBM and the receiving energy level of Eu^{3+} was decreased, which indicated that the absorbed by DBM ligand as an antenna was harder to transfer to Eu^{3+} ion after Fe^{3+} adsorption (Fig. S25 in Supporting information) [29].

In conclusion, luminescence detection of Fe^{3+} ion in water at pmol/L level was realized for the first time. The Fe^{3+} adsorption as single-ion mode onto the Eu-O_8 node greatly inhibited the charge and energy transfer pathways within Eu-DBM molecule, which contributed to the ultrasensitive luminescence detection behavior toward Fe^{3+} ion. In this work, the obtained ultralow LOD and single-ion adsorption mechanism open a door for designing and developing advanced luminescence sensing materials.

Declaration of competing interest

The authors declare that they have no known competing financial interests or personal relationships that could have appeared to influence the work reported in this paper.

Acknowledgments

We thank the National Natural Science Foundation of China (No. 22075071), Harbin Manufacturing Science and Technology Innovation Talent Project (No. 2022CXRCCG016), Outstanding Youth Science Foundation of Heilongjiang University (No. JCL202002) and Special Project of Joint Dairy College in East University of Heilongjiang – National Dairy Engineering and Technology Research Center (No. LHXYDS202001).

Supplementary materials

Supplementary material associated with this article can be found, in the online version, at doi:10.1016/j.cclet.2023.108532.

References

[1] S. Bolisetty, M. Peydayesh, R. Mezzenga, Chem. Soc. Rev. 48 (2019) 463–487.

[2] Z. Bai, X. Ren, Z. Gong, et al., Chin. Chem. Lett. 28 (2017) 1901–1904.
[3] J.J. Pang, R.H. Du, X. Lian, et al., Chin. Chem. Lett. 32 (2021) 2443–2447.
[4] H. Wang, X. Wang, R.M. Kong, L. Xia, F. Qu, Chin. Chem. Lett. 32 (2021) 198–202.
[5] C. Fan, X. Huang, L. Han, et al., Sens. Actuators B: Chem. 224 (2016) 592–599.
[6] J. Qian, N. Cao, J. Zhang, et al., Chin. Chem. Lett. 31 (2020) 2925–2928.
[7] M. Li, B. Gurram, S. Lei, et al., Chin. Chem. Lett. 32 (2021) 1316–1330.
[8] Y.M. Zhang, J.X. He, W. Zhu, et al., Mater. Sci. Eng. C 100 (2019) 62–69.
[9] X. Guo, G. Yue, J. Huang, et al., ACS Appl. Mater. Interfaces 10 (2018) 26118–26127.
[10] S. Wang, B. Sun, J. Sun, et al., Dyes Pigm. 202 (2022) 110256.
[11] X. Zhang, X. Jin, Y. Li, Chin. Chem. Lett. 33 (2022) 2117–2120.
[12] X. Zhang, L. Zhao, X. Jin, Z. Zhang, Y. Li, Anal. Chim. Acta 1181 (2021) 338905.
[13] Y. Li, Y. Ban, R. Wang, et al., Chin. Chem. Lett. 31 (2020) 443–446.
[14] Y. Shi, J. Liu, Y. Zhang, et al., Chin. Chem. Lett. 32 (2021) 3189–3194.
[15] W.M. Chen, X.L. Meng, G.L. Zhuang, et al., J. Mater. Chem. A 5 (2017) 13079–13085.
[16] K. Sheng, H. Lu, A. Sun, et al., Chin. Chem. Lett. 30 (2019) 895–898.
[17] Y. Li, X. Wang, C. Xing, et al., Chin. Chem. Lett. 30 (2019) 1440–1444.
[18] M. Yu, Y. Xie, X. Wang, Y. Li, G. Li, ACS Appl. Mater. Interfaces 11 (2019) 21201–21210.
[19] L.Y. Guo, H.F. Su, M. Kurmoo, et al., ACS Appl. Mater. Interfaces 9 (2017) 19980–19987.
[20] X.P. Wang, L.L. Han, Z. Wang, L.Y. Guo, D. Sun, J. Mol. Struct. 1107 (2016) 1–6.
[21] X. Jin, L. Zhao, X. Zhang, et al., ACS Appl. Mater. Interfaces 14 (2022) 42267–42276.
[22] X.L. Tao, M.C. Pan, X. Yang, R. Yuan, Y. Zhuo, Chin. Chem. Lett. 33 (2022) 4803–4807.
[23] S. Prasad, I. Mandal, S. Singh, et al., Chem. Sci. 8 (2017) 5416–5433.
[24] M. Xie, C. Han, Q. Liang, et al., Sci. Adv. 5 (2019) eaav9857.
[25] R.D. Vecchio, N.V. Blough, Environ. Sci. Technol. 38 (2004) 3885–3891.
[26] Q. Yan, Y. Yang, W. Chen, et al., Chem. Eng. J. 459 (2023) 141585.
[27] Y. Hu, C. Zhao, L. Yin, et al., Chem. Eng. J. 349 (2018) 347–357.
[28] Y. Yang, T. Zou, Z. Wang, et al., Nanomaterials 9 (2019) 738.
[29] H.Q. Yin, X.Y. Wang, X.B. Yin, J. Am. Chem. Soc. 141 (2019) 15166–15173.